FERMILAB-PUB-12-909-APC
ACCEPTED

Experimental study of multichromatic terahertz wave propagation through planar micro-channels

Young-Min Shin*, Anisullah Baig, Robert Barchfeld, Diana Gamzina, Larry R. Barnett, and Neville C. Luhmann Jr

Department of Electrical and Computer Engineering, University of California, Davis, CA 95616, USA

Abstract

Previous theoretical and numerical studies [Y. M. Shin, Appl. Phys. Lett. 92, 092501, and 93, 221504 (2008)] have reported that a planar micro-channel with an asymmetric corrugation array supports strongly confined propagation of broadband THz plasmonic waves. The highly broad spectral response is experimentally demonstrated in the near-THz regime of 0.19 ~ 0.265 THz. Signal reflection and transmission tests on the three designed micro-channels including directional couplers resulted in a full-width-half-maximum (FWHM) bandwidth of ~ 50 -60 GHz with an insertion loss of ~ -5 dB, which is in good agreement with simulation data. These micro-structures can be utilized for free electron beam and electronic/optic integrated devices.

Key word: terahertz, plasmonic, electron beam, micro-channel

* Current Affiliation: Department of Physics, Northern Illinois University, Dekalb, IL, 60115, USA and Accelerator Physics Center (APC), Fermi National Accelerator Laboratory (FNAL), Batavia, IL 60510, USA (e-mail: yshin@niu.edu and youngmin@fnal.gov)

Operated by Fermi Research Alliance, LLC under Contract No. De-AC02-07CH11359 with the United States Department of Energy

Recently, considerable amount of attention has been focused on terahertz (THz) technology[1 – 3] since this spectral regime has invaluable scientific potential due to its unique physical nature. Practically powerful generation and sensitive detection of THz signals have, however, been the most challenging issues due to the absence of an appropriate EM-wave control methodology in the physical limit between electronics and optics[4 – 8]. Various techniques based on optics and solid-state electronics have been adopted; however, the metallic guiding approach is still one of the most efficient ways to control high energy EM flows in the THz regime. In many cases, THz sources and detectors utilize metal RF components such as waveguides and cavities as their resultant energy loss is relatively lower than electronic transport in a medium. In particular, free electron beam coherent radiation sources[9] such as traveling wave tubes and klystrons need to minimize energy losses in order to maximize RF-beam energy conversion. Evanescent wave propagation becomes strongly attenuated if impedance mismatching and/or surface asperity is present along the surface current paths, so that the signal response of confined EM waves can be significantly weakened depending upon frequency-dependent matching condition. Efficient energy transfer of multichromatic plasmons is thus prerequisite for developing THz passive and active devices with high SNR. Most recently, preliminary studies[10 – 13] showed that insertion of staggered double grating arrays into the TE-mode waveguide distorts its dispersion relation, thereby significantly broadening the intrinsic bandwidth. This prior work demonstrated that this structure supports ~ 30 % instantaneous bandwidth with ~10 - 12 dB/cm signal transmission. However, this broadband response has not heretofore been experimentally demonstrated in the THz regime.

This paper presents test results of the proposed slow wave structure (SWS) in the THz region together with comparisons with simulation results. For the experiment, three types of the designed structure are fabricated by microelectromechanical system techniques such as ultraviolet (UV) LIGA (lithography, electroplating, and molding, German acronym)[14 – 16] and ultra-precision nano-machining[17, 18]. The actual field distribution corresponding to the measured frequency points is reproduced by finite-integral-technique simulations[19].

A symmetrically paired grating array in the TE-mode waveguide has an out-of-phase transverse distribution of axial electric fields, E_z, in the fundamental passband (1^{st} plasmonic band) that is decoupled with the electrons. In the structure, the axial fields on the top and bottom gratings cancel each other out, so that the destructive field confinement results in no energy transfer to the electron beam. However, half period staggering of the two grating positions renders the transverse distribution in-phase, which thereby creates constructive field confinement in the axial direction. In Fig. 1(a), the top and bottom vanes shifted off by a half period convert field-orientation of the fundamental (1^{st}) passband in-phase. Simulation modeling analysis in prior work[10 - 13] showed that the polarization shift is ascribed to serpentine motion of the evanescent fields between vanes in the beam channel. In fact, the asymmetry imposes in-phase polarity on the eigenmodes of higher order passbands. Figure 1(b) shows the dispersion relation of the SWS with a 70 GHz FWHM (1^{st}) bandwidth extending from 0.195 THz to 0.265 THz. Basically, the lower cutoff is primarily determined by the waveguide width, *h*. Note that the strong energy localization in the channel significantly reduces ohmic losses and enhances the beam-loading interaction impedance. The impedance rises toward, and in principle goes to, infinity at cutoffs where the group velocities vanish owing to standing wave formation. Multi-chromatic excitation of non-radiative modes in the micro-channel is enabled when characteristic impedance of external loads is matched with the ones of the SWS over the broad bandwidth. Normally, intrinsic wave impedance varies appreciably around the stop-bands, so that coupling efficiency falls off considerably as frequency approaches cutoffs of the forbidden energy bands. Furthermore, sub-wavelength structures become heavily lossy with an increase of frequency since the surface current area is effectively enlarged if structural dimensions are smaller relative to wavelengths (de-homogenization effect), increasing RF ohmic losses. The quasi-optical matching design using asymmetric alignment is thus effective to minimize THz attenuation over a wide spectrum. In the experiments, we tested three types of micro-channels with (a) tapered straight couplers, (b) back-to-back L-shaped directional couplers, and (c) extended L-shaped directional couplers. In the THz regime, structural dimensions of the micro-channels are too small for conventional manufacturing techniques to handle. Consequently, the samples are thus fabricated by UV lithography molding and ultra-precision nano-machining.

Figure 2 shows signal transmission and reflection analysis of (a) the SWS with the tapered straight couplers. Since the coupler is a geometrically two-dimensional structure, the sample was prepared by a UV lithography molding process. As for the sample fabrication, viscous photoresist (KMPR-2150) film is patterned with the circuit features by UV exposure on the copper wafer. Following development, electro-deposition, and mold removal, tall copper structures are constructed. The circuit holder is machined with the straight waveguides. In the design, the 150 μm wide beam tunnel is tapered up toward standard WR-4 waveguide over 5 mm, which thereby enables adiabatic transition of plasmons from the external loads to the interaction circuit. In Fig. 2(b), the experimental transmission graph ends at 0.265 THz which is the upper limit of our scalar network analyzer (SNA), while in simulation the designed dispersion curve (1^{st} and 2^{nd} fundamental passbands) spans 0.295 THz. The 40 mm long circuit only has - 5 ~ 6 dB of insertion loss (S_{21}) and – 7 ~ 8 dB of return loss (S_{11}) over the dispersion curve. The measurements revealed an attenuation of ~ 0.15 dB/mm. The attenuation is relatively small compared to other types of THz SWSs, which is attributed to the strongly localized energy propagation between the staggered grating arrays. Most of the RF current flows along the top and bottom surfaces, which significantly reduces RF ohmic losses (Figure 1(a)). It should be noted that the frequency spectrum of the passband appears to fluctuate with ripples, resulting from noise background in the measurement system. The noise carrier level was noticeably reduced by shielding the connector box. For the experiment, the lower cutoff is designed to be ~ 0.195 THz (height = 385μm). However, fabrication error mainly due to excessive surface-grinding (385μm → 360 ~ 370μm), in addition to residual undercuts and rounded corners in UV lithography process, resulted in slightly smaller waveguide dimensions, which thereby shifts the cutoff up to ~ 0.21 THz. Figure 2(c) shows that the experimental data agree well with the simulation models with ~720 - 740 μm except for the noise fluctuation. Due to the scanning limitation of our SNA system, the stop-band of forbidden photon energy between the 1^{st} and 2^{nd} fundamental bands is not properly presented in the experiment graph (vane tip width tapering for impedance matching). Nevertheless, no detectable error appears in the experimental data. Test results could be improved further by completely shielding all of the electronic components.

THz device elements need to be densely integrated in a small volume, so that they can be configured with complex features such as bends and twists, which can lead to intense energy loss and narrowing of intrinsic matching bandwidth. For the multi-chromatic external coupling of the SWS, we designed an L-bend directional coupler with the tapered vane arrays, as shown in Fig. 3(a), which replaces the straight coupler of Fig. 2(a). Figure 3(a) depicts the back-to-back coupler assembly model for the RF cold test. In the model, the grating height is tapered down toward the bent waveguide connecting with the vertically polarized (TM-mode) oversized beam tunnel waveguide (770 × 1,200 μm^2). The 90°-rotated oversized waveguide plays a role in mismatching the RF impedance toward the outward beam tunnel. The grating height is gradually tapered over 5 vane periods with the optimized dimensions for broadband matching. The coupler is fully three-dimensional and is fabricated by the nano-machine[17, 18]. The ultra-precision machine enables extremely high dimensional accuracy and surface smoothness by using diamond drills to make the vane pockets on the tapered waveguide. The scanning-electron-microscope (SEM) image in Fig. 3(b) indicates that the dimensional accuracy is less than 1 μm and that the surface finish on the sidewall is ~ 100 nm. Note that for the sake of fabrication convenience, the test waveguide sample is machined to be split along the H-plane which coincides with the maximum surface current. The H-plane split of waveguide components ("bad" plane) is uncommon in the manufacturing of commercial waveguides, as electrical segregation of the H-field maximum plane through which most of the RF surface current flows can cause a considerable amount of signal loss. However, diffusion bonding in a hydrogen furnace completely seals up gaps between the two circuit halves, leaving current paths over the sidewall surface intact. In Figs. 3(c) and (d), the experimental reflection and transmission spectra of the experimental data appear to be well matched with simulation data (within ~1 - 2 dB). While the adiabatic transition of the optical impedance of the designed coupler assists in compensating for falloff of the passband at the upper cutoff, the lower-cutoff mismatch results from fabrication errors. Unlike the lithographically fabricated test sample with the rectangular shapes in Fig. 2, the diamond drills left rounded corners on the nano-machined waveguide in Fig. 3, which thereby up-shifts the dynamic spectra by a few GHz. Nevertheless, the experiment agreed very well with the simulation since the numerical model was designed in consideration with the rounded corners.

Figure 4(a) illustrates the fully designed model of the 40 mm long guided THz wave structure with 90 periods of staggered cavities and the input/output couplers. The full micro-channel was also fabricated by ultra-precision nano-machining with < 1 μm dimensional tolerance and < 100 nm surface roughness. The RF response test of the long structure ended up being in excellent agreement with simulation. In Fig. 5, the measured transmission coefficient (S_{21}) is - 3 ~ 5 dB over the passband of ~ 0.205 – 0.28 THz, corresponding to attenuation of only ~ 0.75 – 1.25 dB/cm, while reflection coefficient (S_{11}) roughly ranges from – 15 to 20 dB over the passband. This test result strongly corroborates the contention that imposing asymmetry on the Maxwell-Bloch system allows evanescent optical waves to be non-radiative over an exceptionally broad spectral range. Figure 5(b) (inset) shows that the staggered grating pair induces strongly confined EM energy propagation with S_{21} = ~ - 4.5 dB at 0.22 THz, where ports-1 and -2 are referred to as the input and output ports, respectively. It is noted that the dip emerges at ~ 0.28 THz which is the stop-band at the coalescence mode between the first forward and second backward wave bands, as depicted in Fig. 1(b) (The small dips are just numerical glitches). The broadband coupling efficiency of the designed structure is mainly ascribed to shaping the coupler into an L-bend together with the asymmetrically tapered transition and vertically polarized (90°-rotated) mismatching. This THz plasmonic wave guiding scheme can be utilized for the highly integratable passive and active elements for various electronic and optic devices.

In summary, low loss coupling and propagation of THz plasmonic waves in the micro-channels comprised of directional couplers and asymmetrically corrugated TE-mode waveguides were experimentally demonstrated in the H-band of 0.18 – 0.265 THz. The tests showed that the asymmetric double corrugation supports highly efficient THz coupling and transmission through the micro-channel with the broad spectral coverage in that $S_{21} \leq -5$ dB and FWHM bandwidth ~ 30 %, which agreed significantly well with simulation data. This channel plasmonic structure can be adopted in various electronic and optics devices such as to control THz signals in the integrated photonic and electronic devices or to induce strong beam-wave interaction in free electron beam devices.

Acknowledgements

This work is supported by the HiFIVE (High Frequency Integrated Vacuum Electronics) program of DARPA, Grant No. G8U543366 through a subcontract from Teledyne Scientific.

References

[1] E. R. Muller, Ind. Phys. **9**, 27 (2003)

[2] A. Dobroiu, M. Yamashita, Y. N. Ohshima, Y. Morita, C. Otani, and K. Kawase, Appl. Opt. **43**, 5637 (2004)

[3] D. van der Weide, Opt. Photonics News **14**, 48 (2003)

[4] D. H. Auston, K. P. Cheung, J. A. Valdmanis, and D. A. Kleinman, Phys. Rev. Lett. **53**, 1555 (1984)

[5] J. J. Song, S. Bajikar, F. Decarlo, Y. W. Kang, R. L. Kustom, D. C. Mancini, A. Nassiri, B. Lai, A. D. Feineman, and V. White, Microsyst. Technol. **4**, 193 (1998)

[6] G. Scheitrum, G. Caryotakis, A. Hasse, L. Song, B. Arfin, Y. Cheng, B. Shew, and B. James, AIP Conf. Proc. **569**, 712 (2001)

[7] J. Faist, F. Capasso, D. L. Sivco, C. Sirtori, A. L. Hutchinson, and A. Y. Cho, Science **264**, 553 (1994)

[8] C. Fattings and D. Grischkowsky, Appl. Phys. Lett. **54**, 490 (1989)

[9] Robert K. Parker, Richard H. Abrams, Bruce G. Danly, Baruch Levush, IEEE Trans. Micro. Theo. Tech. 50, 835 (2002)

[10] Young-Min Shin, Larry R. Barnett, and Neville C. Luhmann Jr., Appl. Phys. Lett. 93, 221504 (2008)

[11] L. R. Barnett and Y. M. Shin, US Patent Application No. 60979392, Oct. 12 (2007)

[12] Young-Min Shin, Larry R. Barnett, and Neville. C. Luhmann. Jr., IEEE Trans. Elec. Dev. 56(12), 3196 (2009)

[13] Young-Min Shin and Larry R. Barnett, Appl. Phys. Lett. 92, 091501 (2008)

[14] V. White, R. Ghodssi, C. Herdey, D. D. Denton, and L. McCaughan, Appl. Phys. Lett. **66**, 2072 (1995)

[15] Young-Min Shin, Jin-Kyu So, Seong-Tae Han, Kyu-Ha Jang, Gun-Sik Park, Jong-Hyun Kim, and Suk-Sang Chang Appl. Phys. Lett. **88**, 091916 (2006)

[16] Yong-Seok Kim, Seong-Cho Yu, Hong Lu, Jeong-Bong Lee, and Heebok Leea, J. Appl. Phys. **99**, 08B309 (2006)

[17] Young-Min Shin, Jinfeng Zhao, Larry R. Barnett, and Neville C. Luhmann Jr., **Phys. Plasmas 17,** 123105 (2010)

[18] Robert A. Barchfeld, Diana Gamzina, Young-Min Shin, Jongsoo Kim, Christopher Alldritt, Larry R. Barnett, and Neville C. Luhmann, 26th Annual Meeting of the American Society for Precision Engineering (ASPE), Denvor, CO, USA

[19] CST Microwave Studio version 2011

Figure Captions

FIG. 1 (a) Asymmetrically corrugated planar micro-channel with dimensional parameters (RF current distribution on the conductor surface) (b) dispersion curves of 1st and 2nd fundamental plasmonic bands in spatial harmonics

FIG. 2 (a) SEM images of UV-fabricated sample (with the straight coupler) (b) measured reflection (S_{11}) and transmission (S_{21}) graphs (c) transmission graphs of experiment and simulations with respect to the channel heights of 360 μm and 370 μm.

FIG. 3 (a) Back-to-back assembly model of the L-bend directional couplers (b) SEM image of the test sample fabricated by nano-machining (c) transmission (S_{21}) and (d) reflection (S_{11}) graphs from experiment and simulation

FIG. 4 (a) 40 mm long SWS model with the L-bend directional couplers (b) and (c) SEM images of the test sample fabricated by nano-machining

FIG. 5 (a) Reflection (S_{11}) and (b) transmission (S_{21}) graphs from experiment and simulation (inset is the electric field distribution)

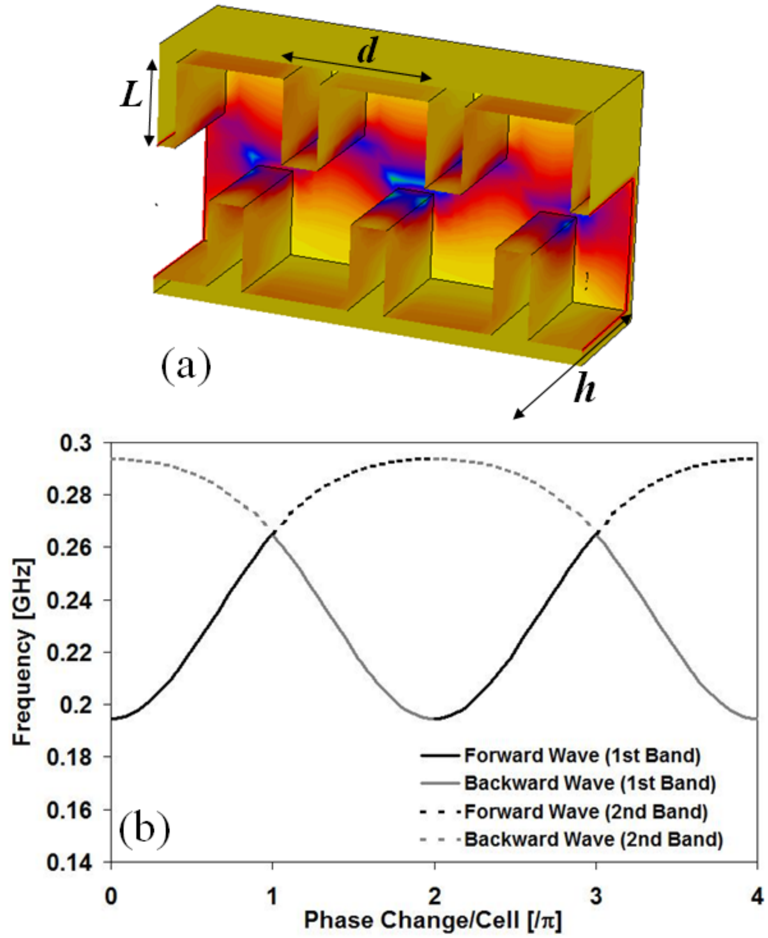

FIG. 1 (Y. M. SHIN)

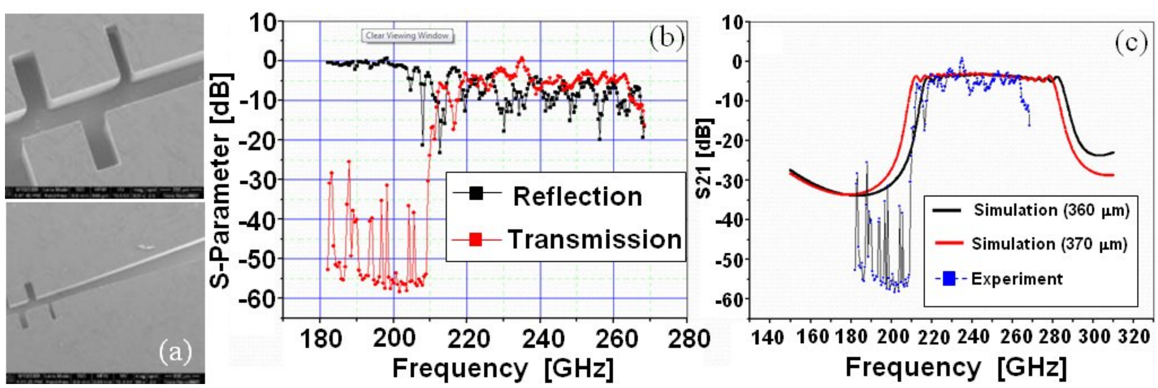

FIG. 2 (Y. M. SHIN)

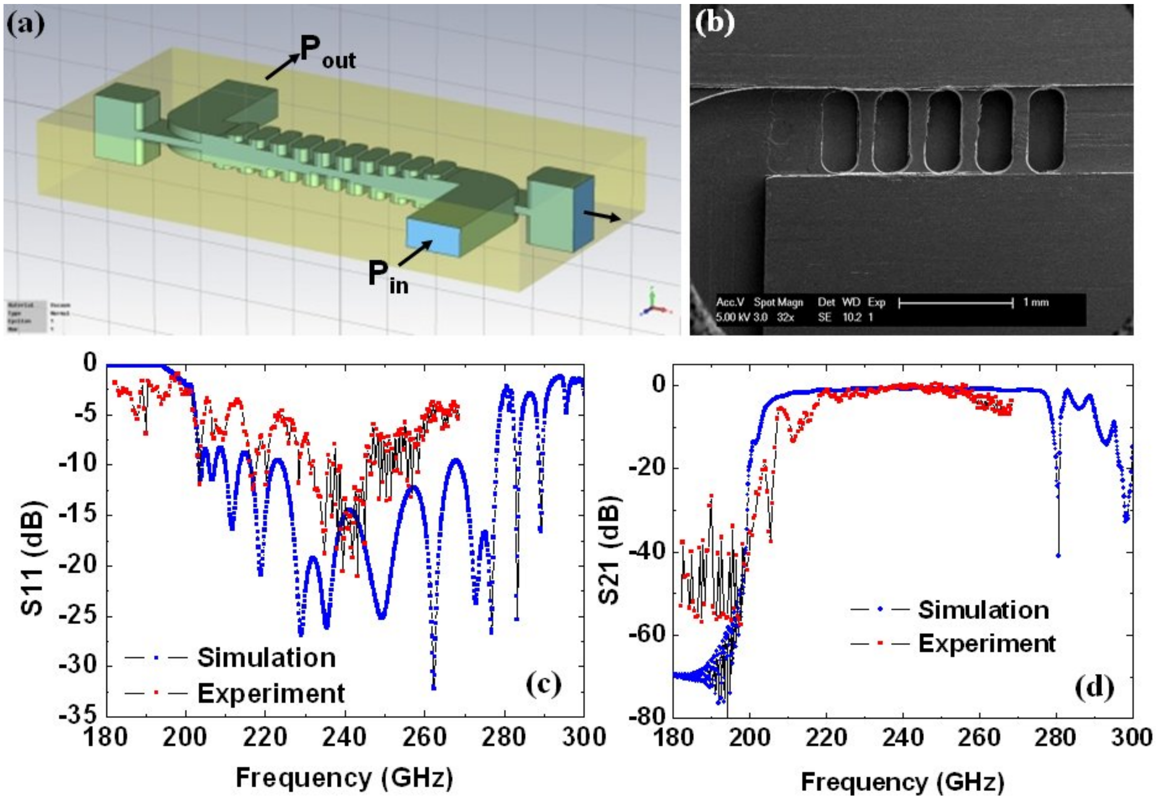

FIG. 3 (Y. M. SHIN)

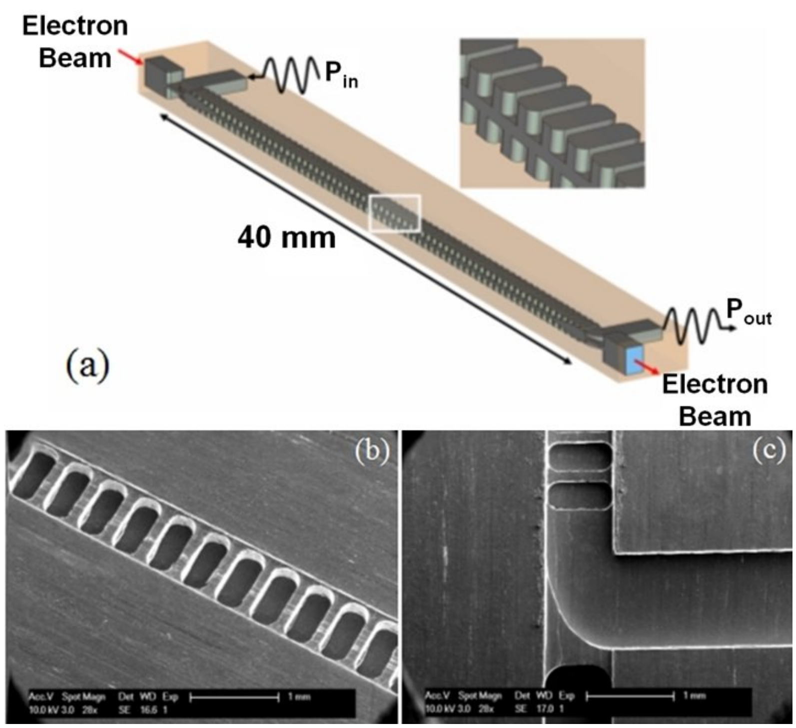

FIG. 4 (Y. M. SHIN)

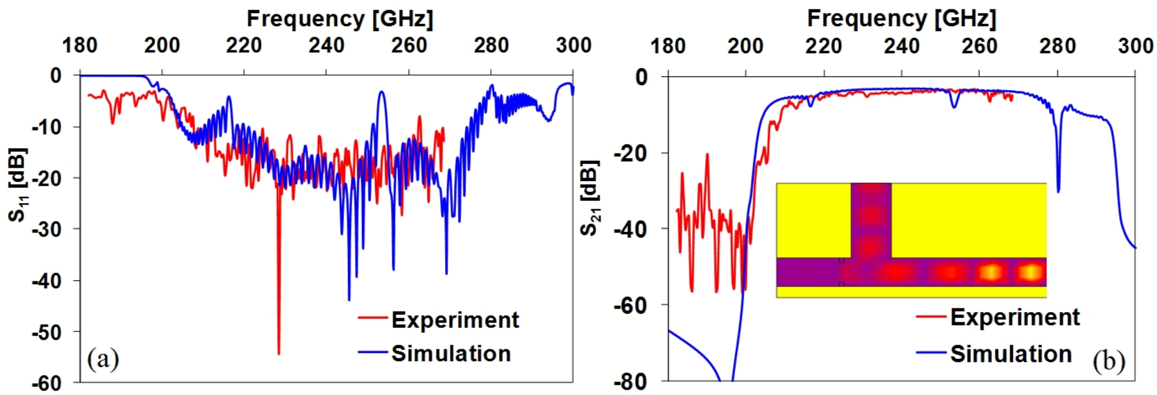

Frequency [GHz]
180
200
220
240
260
280
300
0
-10
-20
-30
-40
-50
-60
S11 [dB]
Experiment
Simulation
(a)
Frequency [GHz]
180
200
220
240
260
280
300
0
-20
-40
-60
-80
S21 [dB]
Experiment
Simulation
(b)

FIG. 5 (Y. M. SHIN)